Two-dimensional to bulk crossover of the WSe2 electronic band structure

Raphaël Salazar, Matthieu Jamet, Céline Vergnaud, Aki Pulkkinen, François Bertran, Chiara Bigi, Ján Minár, Abdelkarim Ouerghi, Thomas Jaouen, Julien Rault, et al.

Two-dimensional to bulk crossover of the WSe_2 electronic band structure

IOP Publishing Electron. Struct. 7 (2025) 025008 https://doi.org/10.1088/2516-1075/addca9

Electronic Structure

OPEN ACCESS

RECEIVED
21 March 2025

REVISED
7 May 2025

ACCEPTED FOR PUBLICATION
23 May 2025

PUBLISHED
10 June 2025

PAPER

Two-dimensional to bulk crossover of the WSe_2 electronic band structure

Raphaël Salazar[1,2], Matthieu Jamet[3], Céline Vergnaud[3], Aki Pulkkinen[2], François Bertran[1], Chiara Bigi[1], Ján Minár[2], Abdelkarim Ouerghi[4], Thomas Jaouen[5], Julien Rault[1,6] and Patrick Le Fèvre[1,5,*]

[1] Synchrotron SOLEIL, L'Orme des Merisiers, Départementale 128, F-91190 Saint-Aubin, France
[2] New Technologies Research Centre, University of West Bohemia, 30100 Pilsen, Czech Republic
[3] Univ. Grenoble Alpes, CEA, CNRS, Grenoble INP, IRIG-SPINTEC, 38000 Grenoble, France
[4] Université Paris-Saclay, CNRS, Centre de Nanosciences et de Nanotechnologies, 91120 Palaiseau, Paris, France
[5] Univ Rennes, CNRS, IPR—UMR 6251, F-35000 Rennes, France
[6] ABB Switzerland Ltd, Baden Dättwil, Switzerland
[*] Author to whom any correspondence should be addressed.

E-mail: patrick.lefevre@univ-rennes.fr

Keywords: transition metal dichalcogenides, 2D-materials, ARPES, molecular beam epitaxy

Supplementary material for this article is available online

Abstract

Transition metal dichalcogenides (TMDs) are layered materials obtained by stacking two-dimensional sheets weakly bonded by van der Waals interactions. In bulk TMD, band dispersions are observed in the direction normal to the sheet plane (z-direction) due to the hybridization of out-of-plane orbitals but no k_z-dispersion is expected at the single-layer limit. Using angle-resolved photoemission spectroscopy, we precisely address the two-dimensional to three-dimensional crossover of the electronic band structure of large area epitaxial WSe_2 thin films. Increasing number of discrete electronic states appears in given k_z-ranges while increasing the number of layers. The continuous bulk dispersion is nearly retrieved for 6-sheet films. These results are reproduced by calculations going from a relatively simple tight-binding model to a sophisticated KKR-Green's function calculation.

1. Introduction

Ever since the discovery of graphene [1, 2], research on two-dimensional (2D) materials is ongoing a tremendous effort. Along with this trend, transition metal dichalcogenides (TMDs) are extremely promising for possible technological applications. Their general formula is MX_2, where M is a transition element and X is a chalcogene. Those two elements form a MX_2 basic layer, where M atoms are sandwiched between two covalently-bonded planes of chalcogenes. The three-dimensional (3D)-solid is obtained by stacking these X–M–X sheets, only weakly bonded by van der Waals interactions [3], conferring to TMD a very pronounced 2D-character. Nowadays, research pushes towards increasingly elaborated structures taking advantage of the 2D nature of these materials: twisted TMD layers [4, 5], hybrid TMD structures (e.g. $MoSe_2/WSe_2$, WS_2/WSe_2) [6–8] or alloyed TMD systems [9–11]. In the ideal case, these structures are studied by angle-resolved photoemission spectroscopy (ARPES), a technique which allows for direct measurement of the band structure. Its surface sensitivity makes it particularly well-suited to probe 2D-compounds. For bulk TMD-crystals, despite the expected strong 2D-nature of these materials, a significant band dispersion can be observed perpendicular to the MX_2-sheets [12–14]. As a matter of fact, both the M-d_{z^2} and the X-p_z orbitals (the z-axis being perpendicular to the MX_2-sheets) point out from the MX_2-planes and can hybridize to give rise to this perpendicular dispersion. It can be successfully modeled either using density functional teory [13] or a tight-binding approach [14]. At low thickness, the calculations presented in [15] show that each new layer in the stacking generates an additional band at Γ. Figure 1 shows dispersions measured on a 2-layer WSe_2 sample in directions parallel to $\Gamma - K$ for various photon energies, i.e. various position along the $\Gamma - A$ direction. We do observe the expected two bands at 31 and 51 eV-photon energies, but not at 21 and 42 eV.

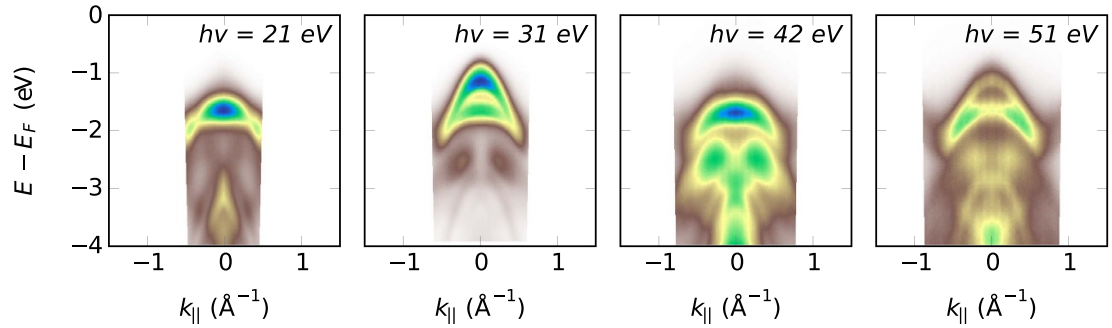

Figure 1. ARPES on 2-layer WSe_2 giving the band-dispersion in directions parallel to $\Gamma - K$ at various photon energies (21, 31, 42 and 51 eV, from left to right). Depending on the photon energy, one or two bands are visible at Γ between −2 eV binding energy and the Fermi level. Spectra have been symmetrized with respect to Γ.

That means that even for ultimately thin samples, 'k_z -effects', or at least, photon energy-dependent intensity of the electronic states associated to out-of-plane electronic states can be expected in connection with state discretization as the thickness of the film decreases. Previous work on single and bi-layer MoS_2 [16] or WSe_2 [5] already hinted at those conclusions without proposing a complete explanation. These primary observations urge towards a better understanding of the k_z-dependence even for thin samples.

We propose here to study the transition from the 2D-electronic structure of an ultimately thin TMD to a 3D-bulk crystal. We focus on WSe_2, whose electronic structure has already been extensively scrutinized [13–15]. The perpendicular dispersion of the band structure is measured by ARPES for sample thicknesses of 2, 3 and N (=6–7) layers. The 2- and N-layer samples were grown by molecular beam epitaxy (MBE) on graphene/SiC (Gr–SiC). To complete the experiment, a 3-layer sample of WSe_2, grown on Mica and then wet-transferred onto a Gr–SiC substrate [17] (prepared for another experiment [18]) was also used. We insist on the fact that epitaxial WSe_2 films are homogeneous at the cm^2 scale. More details about the samples are given in the supplementary material.

2. Methods

2.1. Samples

Most of the samples were grown by MBE on graphene/SiC(0001), held at 573 K as measured by a thermocouple in contact with the sample holder) by co-evaporating W from an e-gun evaporator at a rate of 0.15 Å min^{-1} and Se from an effusion cell. The Se partial pressure measured at the sample position is fixed at 10^{-6} mbar. *In situ* reflection high energy electron diffraction is used to monitor the WSe_2 crystal structure during growth. The obtained WSe_2 films were then annealed at 1023 K during 15 min to improve the crystalline quality. Using this method, centimeter scale (here typically 1×1 cm^2) samples can be obtained with a precise control of their thickness, given by the amount of deposited W, Se atoms being in excess by a factor ∼20 [17, 19, 20]. Prior to their introduction in the ARPES chamber, the samples were annealed at 573 K until the pressure stabilized and reached down $P \simeq 10^{-9}$ mbar (about three hours). The annealing aimed to eliminate most of the contamination adsorbed on the surface. More details about the sample growth and characterization can be found in the supplementary material.

2.2. ARPES measurements

The ARPES measurements were all performed at the CASSIOPEE beamline of the SOLEIL storage ring using a Scienta R4000 analyzer. All the measurement were performed at room temperature. The samples were first aligned with the $\Gamma - K$ direction of WSe_2 reciprocal lattice along the entrance slit of the analyzer. We call $k_{||}$ the component of the wave vector parallel to this direction. A ($k_{||}$, E_B) image can then be measured at once thanks to the 2D-detector of the electron analyzer. Here, E_B is the electron binding energy; it is measured with respect to the Fermi level E_F. k_z was changed by scanning the photon energy from 20 to 90 eV (by 1 eV-step), which amounts to span a k_z-range from roughly 2.5 to 5 $Å^{-1}$. The principle of the monochromator installed on CASSIOPEE does not allow for an absolute determination of the photon energy. To calculate the relative binding energies from one measurement to the other as precisely as possible, the Fermi level energy was measured every 5 eV (at 20, 25, ... and 90 eV photon energies) on the Mo-clips holding the sample and connecting it to the ground. More details about the experimental geometry, sample alignment or the determination of the Fermi level can be found in the supplementary material. The data analysis was performed with the CassioPy package available at https://gitlab.com/SLZ_Raph/cassiopy.

2.3. Tight binding calculations

To model our experimental data, we developed a tight-binding model on increasingly thick WSe_2, retaining only the essential physics of the system and inspired by the derivations presented in [21] and [14]. Γ-states are principally composed of one W-5d_{z^2} and two Se-4p_z orbitals. To construct the tight-binding matrix, we use the states $|4p_z^{b(t)}(\mathbf{r}_{b(t),n})\rangle$ with index $b(t)$ corresponding to bottom (top) Se-atoms at position $\mathbf{r}_{b(t),n}$ inside a given layer n, as well as the $|5d_{z^2}(\mathbf{r}_{d,n})\rangle$ states of the W-atom located at position $\mathbf{r}_{d,n}$. More details about the derivation are given in the supplementary material. The code is available at https://gitlab.com/SLZ_Raph/arpestb.

2.4. Spin-polarized relativistic Korringa–Kohn–Rostoker (SPRKKR) calculations

The structures of the 1-, 2- and 3-layer as well as bulk WSe_2 were constructed using the bulk lattice parameters ($a = 3.282$ Å, $c = 12.96$ Å). The electronic structure was calculated using the full potential SPRKKR method (SPRKKR package) [22], which solves the Dirac equation using multiple scattering and Green's functions. The 1-, 2-, and 3-layer structures were solved within a repeated slab geometry with vacuum thickness >25 Å. Exchange and correlation effects were treated at the level of local spin density approximation and the basis set was truncated at $l_{\max} = 3$. The ARPES calculations were performed in layer-KKR formalism with a semi-infinite surface construction. For the 1-, 2-, and 3-layer structures, we set the bulk repeat sequence as vacuum, and therefore the ARPES calculation treats them as truly freestanding thin films.

3. Results

Figure 2 shows a series of ARPES-images recorded on the N-layer sample showing the dispersion along $k_{\parallel}$ for chosen photons energies between 20 and 90 eV. It clearly evidences large variations of the band structure along $\Gamma - A$ (see figure 3(a) for a view of the reciprocal space). The vertical black line is at $k_{\parallel} = 0$. To have a clear view of the k_z-dispersion along $\Gamma - A$, we plot this cut at $k_{\parallel} = 0$ as a function of the perpendicular component of the wave vector on figure 3 for the different samples (same data as a function of the photon energy are available in the supplementary material). Figures 3(b)–(d) show the raw data for 2, 3 and N-layers samples. For the 2-layer sample, the two bands which are the closest to the Fermi level clearly have a discontinuous k_z-dispersion. It consists in linear segments corresponding to k_z-values where these bands appear at $k_{\parallel} = 0$ in the $\Gamma - K$ dispersion. Hence, the top band is visible only for k_z between 3.1 and 3.5 Å^{-1} (photon energies between 23 and 40 eV); it then disappears to show up again between 4 and 4.6 Å^{-1} (50 and 70 eV). It has a low intensity from 4.5 to 5 Å^{-1} (70–80 eV) and becomes bright again from 5 Å^{-1} onward (85 to 90 eV). It therefore appears and disappears when varying the photon energy, confirming the first observations made on figure 1. Near, e.g. $k_z = 3$ or 3.7 Å^{-1} (20 eV and 43 eV) applying the rule one layer = one band at Γ, the sample is indistinguishable from a monolayer system with only one visible band at Γ. Let us note that this is the case around 21 eV, the photon energy produced by He-lamps. The same phenomenon is observable on the 3-layer sample with instead three bands appearing and disappearing. We note that the binding energies are slightly shifted in the 3-layer sample with respect to the 2-layer sample. This derives from the different thicknesses of the Gr–SiC substrate which induce differentiated charge transfers [23]. The reader can find more details in the supplementary material. Nevertheless, the bright segments are shorter in photon energy and more numerous for each band. It starts to draw the clear band oscillations that we clearly see in the N-layer case, where the observed dispersion compares well with previously measured data on bulk-WSe_2 [13, 14]. The same observations can be made on the second derivative images (figures 3(e)–(g)). Contrary to what was previously observed in NbS_2 [24], the quantized levels at Γ due to the finite number of WSe_2 sheets are not resolved in our experiment although figure 3(g) reveals more clearly the discrete states of the N-layer sample. We cannot exclude the presence of higher thickness WSe_2 in the film and thermal broadening could also play a role. Nevertheless, at this thickness the same quasi-bulk k_z-dispersion is observed in MoS_2 [24].

4. Discussion

At these very small thicknesses, the electronic states considered here can certainly be seen as 2D-electronic systems, confined within the few atomic layers forming the WSe_2-film. They can then be described as quantum well states whose behavior in ARPES has been extensively described. The pioneering work of Louie *et al* [25] was the first to evidence intensity variations of the Cu(111) Schockley surface state when varying the photon energy, with maxima for k_z-final states corresponding to L-points of the 3D Brillouin zone. Intensity resonances of surface states using photon energies matching vertical transitions at high symmetry points of the 3D Brillouin zones was later confirmed by, e.g. studies on the Al(001) [26] or Cu-vicinal surfaces [27]. This is precisely what we observe here, although with some complications coming from the

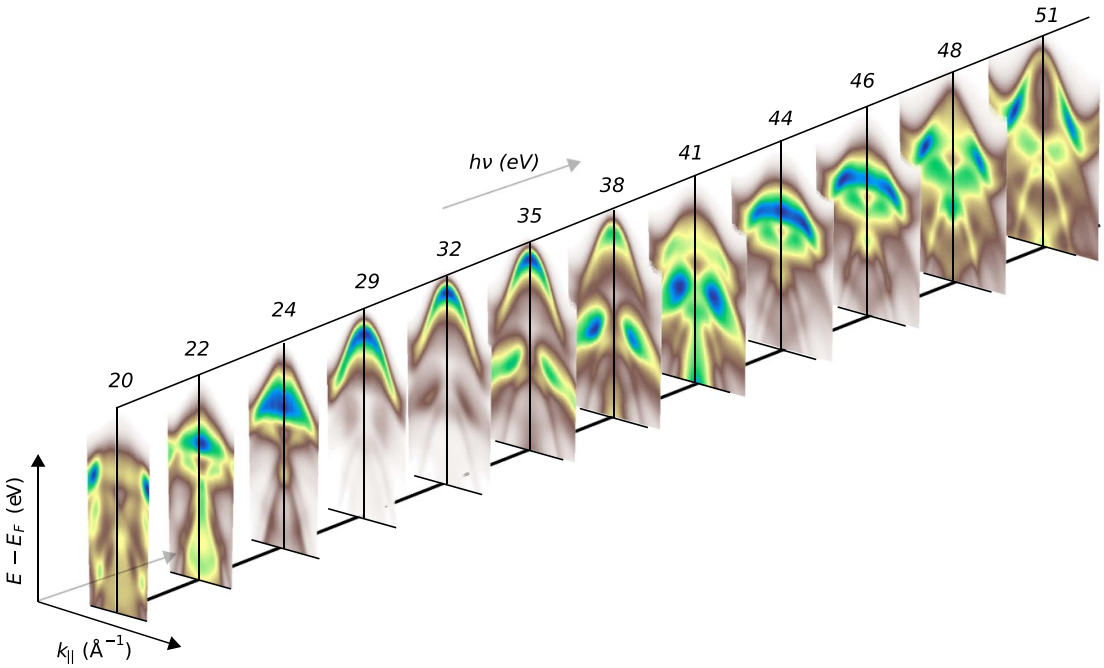

Figure 2. Series of ARPES-images recorded on the N-layer ($N = 6$–7) WSe_2/Gr–SiC sample showing the dispersion along $k_{||}$ for chosen photon energies between 20 and 90 eV. The vertical black line is at $k_{||} = 0$. Similar figures for 2 and 3-layer samples are available in supplementary material.

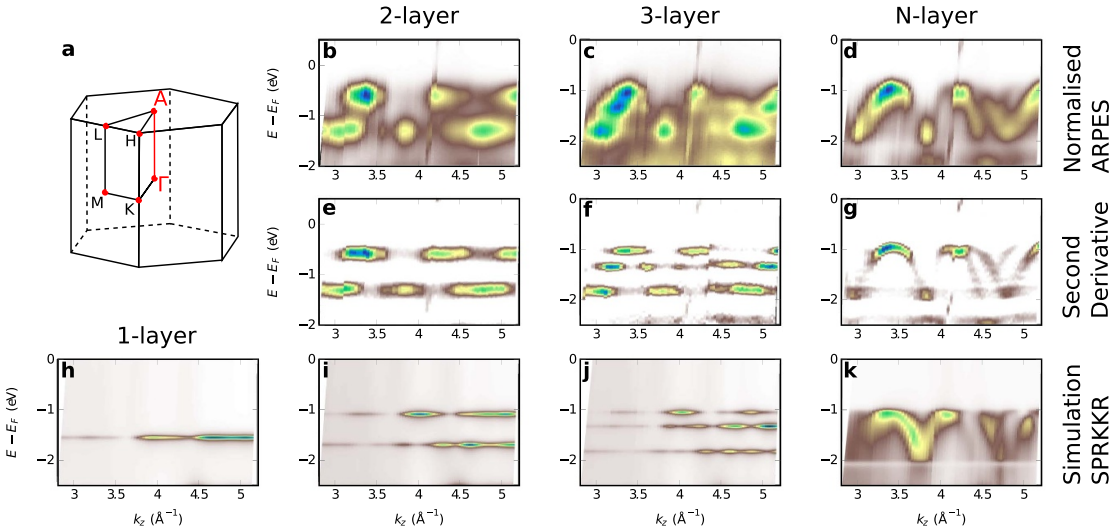

Figure 3. (a) First Brillouin zone of the WSe_2 reciprocal space. (b)–(g) Experimental band intensity variations at Γ along the $\Gamma - A$ direction of the reciprocal space for 2 (left), 3 (middle) and N (right) layers of WSe_2. Panels (b)–(d) show the raw data and panels (e)–(g) their second derivative. Panels (i)–(k) show the corresponding calculations done in the KKR-Green's function formalism (see text for details) with an additional calculation for 1-layer WSe_2 (h). The $h\nu$ to k_z conversion was done using an inner potential V_0 of 13 eV for all spectra (see supplementary material).

WSe_2 crystallographic structure. Taking a c-parameter of 12.96 Å [28], one obtains a $\Gamma - A$ distance of 0.2424 $Å^{-1}$. At low thicknesses (2 and 3-layer samples), the maxima observed in our data (around 3.15, 3.3, 3.8, 4.12 or 5.1 $Å^{-1}$) all correspond to positions either of A- or Γ-points of the reciprocal space. These maxima are observable on all the samples. The periodicity appears therefore as doubled in the reciprocal space, as compared to what is expected. This has been explained by Finteis *et al* [12], following the works of Pescia *et al* [29]. WSe_2 has a hexagonal structure whose primitive cell contains two WSe_2-layers (2H-WSe_2). It belongs to the D^4_{6h}-space group which is nonsymmorphic, i.e. it includes a screw axis which is located in the center of the unit cell along the c-axis. Group theory implies selection rules for photoemission from the Bloch states on the $\Gamma - A$ line of the Brillouin zone that are restricted to the subgroups of Δ_1 and Δ_2

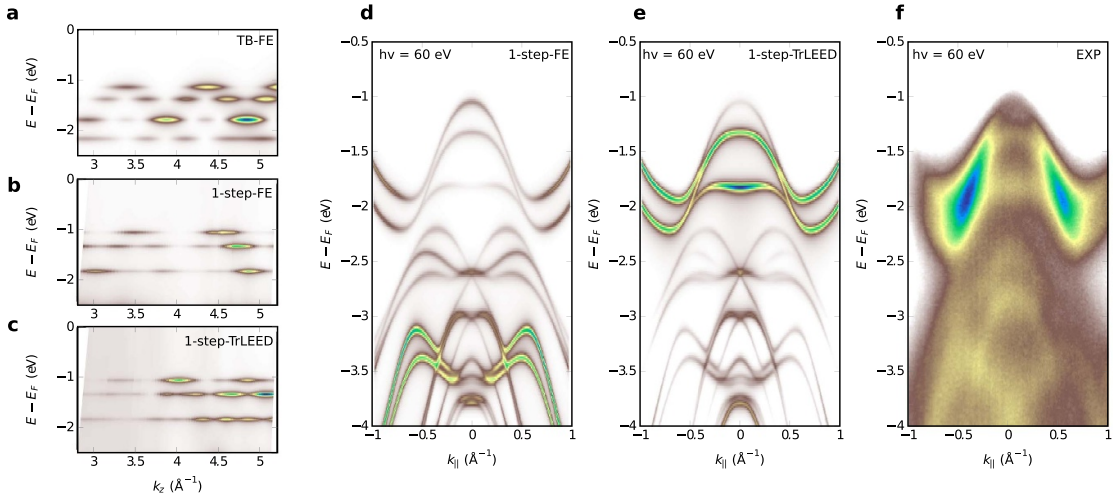

Figure 4. k_z-dispersions for the 3-layer system (a) from tight-binding initial state and free electron final state model (TB-FE), (b) from KKR-Green's function initial state and free electron final state (1-step-FE), (c) from KKR-Green's function initial state and time-reversed LEED final state (1-step-TrLEED). (c) is normalized to the background intensity. 3-layer sample ARPES dispersion at Γ for $h\nu = 60$ (d) calculated in the 1-step-FE model, (e) from the 1-step-TrLEED model and (f) as measured by ARPES. No normalization of intensities have been applied for (d)–(f).

symmetry, respectively, which together with the even parity required for coupling to a free-electron final state, results to allowed optical transition from a given initial state every other Brillouin zone [12].

Our results look very much alike what was obtained on graphene by Ohta *et al* [30]. On a single layer sample, they showed that the π-orbital (forming the famous Dirac cone at the K-point of the reciprocal space) is confined in the crystal plane and show no k_z-dispersion. As the number of graphene layers increases, the number of π-orbital increases because of interlayer interactions and more and more discrete states appear, gradually converging towards the final 3D-dispersion [30]. This is clearly the model system to which our data on WSe_2 should be compared. An apparent doubling of the reciprocal space periodicity is also observed, since graphite structure also belongs to a nonsymmorphic space group [29]. The interpretation of these results was nicely revisited by Strocov in 2018 [31]. In this work, ARPES is first interpreted in a Fourier-transform formalism and quantum confined 2D-states are introduced as standing waves multiplied by an envelope function quickly decreasing away from the surface. This lucid model not only confirms that intensity maxima should appear in ARPES at high symmetry points along k_z, but also predicts that these maxima spread over a k_z-range inversely proportional to the z-spatial extension of the 2D-state [31]. In other words, the 'dots' observed at fixed binding energies should gradually shorten as the z-delocalization increases. This is what is observed on graphene [30] as well as in our results. Finally, let us note that this intensity behavior is also well-reproduced by tight-binding calculations performed on a one-dimensional atomic chain of increasing length [32]. Compared to graphene, our measurements on WSe_2 involve more complicated layers, with two atom-types and different orbital natures ($2p$ or $5d$). In this sense, it is a step forward in the comprehension of the 2D to 3D crossover in these layered systems.

To understand better its physics, we propose to study the system at different levels of approximation using first a tight-binding initial state and free electron (FE) final state (TB-FE model). We then increase the complexity by describing the photoemission process within the one-step model of photoemission [33] as implemented in the SPRKKR package [22] using a FE final state (1-step-FE model). The last step is the calculation using the one-step model and a time-reversed LEED (TrLEED) final state (1-step-TrLEED model). This last result is presented in figures 3(h)–(k) for free-standing 1, 2, 3 and an infinite number of WSe_2 layers. They are in excellent agreement with the measured data, reproducing the discontinuous patterns and converging to a bulk-like dispersion.

The tight-binding model [34] is inspired from the derivation made in [14] and [21]. We aim at a minimal model valid at Γ along the k_z direction. For more complete derivations, the reader can refer to [21, 35–38]. More details about our tight-binding model and the calculation of the photoemission current can be found in the supplementary material. Figure 4 shows the results of the three types of calculation on the trilayer system. In figure 4(a), we see that the simple tight-binding model already captures the essential characteristics of the system with discrete energy states appearing in k_z-ranges in a staggered fashion. It underestimates the total amplitude of the dispersion (difference between the lowest level and highest energy level) of 0.2 eV (see supplementary material for a quantitative comparison of these energy differences at Γ

and K). The intensities are only indicative and the model does not resolve the complex symmetry effects due to the screw-axis [12]. For this reason, we only show the contribution of the phase corresponding to the dominant photoemission intensity in experiments ($\varphi = 2\pi/c$, $c/2$ being the interlayer distance, see supplementary material). Figure 4(b) shows the results for the 1-step-FE model. They are strikingly similar to those of the TB-FE model. They nevertheless show a better agreement with experimental data: the values of the energy levels are more precisely calculated (with discrepancies smaller than 20 meV) and the photoemitted intensity displays additional modulation along k_z. The symmetry effects due to the crystal space group are now consistent with the experimental data. The pattern matches especially well with the measurements in the 2.5–4 Å^{-1} k_z-range. Finally, figure 4(c) shows the outcome of the 1-step-TrLEED model. In essence, the modulation of intensity is a step closer to experimental data. The k_z-patterning matches extremely well the experiment in the 3.5–5.5 Å^{-1} range. On the other hand, we notice a discrepancy with an excess intensity for wavevectors larger than 4.5 Å^{-1} for the top band at -1 eV. Comparing ARPES dispersions along $\Gamma - K$ in figures 4(d) and (e), we see that the 1-step-FE model grossly overestimates the spectral weight of lower energy bands compared to those at the top of the valence bands. In the 1-step-TrLEED, the distribution of the spectral weight is improved: the top of the valence bands generally has a higher intensity than the lower lying bands in the experimental data (see figure 4(f)). A more quantitative comparison of the different models (absolute energy positions of the bands, energy splitting of the bands at Γ, band gaps…) is presented in the supplementary material.

5. Conclusion

The ARPES study of MBE-deposited WSe_2 films with variable thickness gives an overview of the evolution of the electronic structure of this TMD during its transition from 2D to 3D. The behavior observed at thicknesses as low as 2 or 3-layer WSe_2, with discrete states appearing at constant binding energies over finite k_z-ranges, are coherent with the predicted signature of 2D-states, confined in the plane of the atomically-thin crystal. Their evolution with an increasing number of layers shows a larger and larger delocalization as interlayer electronic hoppings become possible. A 6–7 layer thick film already shows an electronic structure comparable to what was measured on bulk crystals. Phenomenological [31] or simplified [32] models, as well as what is usually observed in 2D surface states account well for our measurements. They are similar to what was previously observed on graphene layers [30], although obtained on a more complicated crystallographic system involving several atoms and orbital natures. Here, the results were completely modeled by various methods with increasing complexity: a simple tight-binding model accounts for most of the experimental observations but does not capture the effects of the crystal symmetry on the photoemission signal. An *ab initio* calculation in the KKR-Green's function formalism using a FE final state is more accurate but fails to reproduce the observed relative intensities of the different bands. A similar calculation using a TrLEED final state improves this aspect a lot. These last two calculations are performed on systems with the real geometry, going from 2D to 3D. The electronic properties of TMD, e.g. the nature (indirect or direct) of their band gap, strongly vary with thickness, both in 'classical' TMD [39, 40], or in more sophisticated but close compounds [9]. It is therefore of prime interest to know how the electronic structure evolves, as described by our results. More practically, our work is also a strong warning for those trying to evaluate the thickness of thin TMD samples [5] using ARPES: the photon energy should be chosen carefully. This also applies to calculations performed on such materials close to the monolayer limit, where k_z should be taken into account. Transport measurements average on the whole Brillouin zone and hence on all k-values but they should be sensitive to this k_z-discretization effect which changes the density of states at the top of the valence band. Last, the case of twisted-TMD bilayers is of great interest. Indeed, depending on the twist angle, the interlayer hybridization should change drastically and the k_z-scans proposed here (or in [5]) could be a probe of these variations. As we demonstrated that calculations methods like KKR-Green's function formalism are quite accurate, a predictive approach should be possible.

Data availability statement

All data that support the findings of this study are included within the article (and any supplementary files).

Acknowledgments

R S acknowledges the support of the French National Research Agency (ANR) (CORNFLAKE project, ANR-18-CE24-0015-01). T J and P L F also acknowledge the support of the ANR (MOSAICS project, ANR-22-CE30-0008). This work was supported by the project Quantum materials for applications in sustainable technologies (QM4ST), funded as Project No. CZ.02.01.01/00/22_008/0004572 by Programme

Johannes Amos Commenius, call Excellent Research. This publication was supported by the project TWISTnSHINE, funded as Project No. LL2314 by Programme ERC CZ.

ORCID iDs

Raphaël Salazar https://orcid.org/0000-0001-8240-5914
Matthieu Jamet https://orcid.org/0000-0002-8247-4677
Aki Pulkkinen https://orcid.org/0000-0002-4339-6928
Thomas Jaouen https://orcid.org/0000-0001-5844-5385
Patrick Le Fèvre https://orcid.org/0000-0001-9800-8059

References

[1] Novoselov K S, Geim A K, Morozov S V, Jiang D, Zhang Y, Dubonos S V, Grigorieva I V and Firsov A A 2004 Electric field effect in atomically thin carbon films *Science* **306** 666–9
[2] Novoselov K S, Jiang D, Schedin F, Booth T J, Khotkevich V V, Morozov S V and Geim A K 2005 Two-dimensional atomic crystals *Proc. Natl Acad. Sci.* **102** 10451–3
[3] Dickinson R G and Pauling L 1923 The crystal structure of molybdenite *J. Am. Chem. Soc.* **45** 1466–71
[4] Gatti G *et al* 2023 Flat Γ moiré bands in twisted bilayer WS_2 *Phys. Rev. Lett.* **131** 046401
[5] Parashar B *et al* 2023 Photoemission study of twisted monolayers and bilayers of WSe_2 on graphite substrates *Phys. Rev. Mater.* **7** 044004
[6] Yuan L, Zheng B, Kunstmann J, Brumme T, Kuc A B, Ma C, Deng S, Blach D, Pan A and Huang L 2020 Twist-angle-dependent interlayer exciton diffusion in WS_2–WSe_2 heterobilayers *Nat. Mater.* **19** 617–23
[7] Stansbury C H *et al* 2021 Visualizing electron localization of WS_2/WSe_2 moiré superlattices in momentum space *Sci. Adv.* **7** eabf4387
[8] Khalil L *et al* 2022 Hybridization and localized flat band in the WSe_2/$MoSe_2$ heterobilayer *Nanotechnology* **34** 045702
[9] Ernandes C *et al* 2021 Indirect to direct band gap crossover in two-dimensional $WS_{2(1-x)}$ Se_{2x} alloys *npj 2D Mater. Appl.* **5** 1–7
[10] Vélez-Fort E, Mallet P, Boukari H, Marty A, Vergnaud C, Bonell F, Jamet M and Veuillen J-Y 2022 Alloying two-dimensional VSe_2 with Pt: from a charge density wave state to a disordered insulator *Phys. Rev. B* **106** 075432
[11] Vélez-Fort E *et al* 2022 Ferromagnetism and Rashba spin-orbit coupling in the two-dimensional (V,Pt)Se_2 alloy *ACS Appl. Electron. Mater.* **4** 259–68
[12] Finteis T *et al* 1997 Occupied and unoccupied electronic band structure of WSe_2 *Phys. Rev. B* **55** 10400–11
[13] Riley J M *et al* 2014 Direct observation of spin-polarized bulk bands in an inversion-symmetric semiconductor *Nat. Phys.* **10** 835–9
[14] Kim B S, Rhim J-W, Kim B, Kim C and Park S R 2016 Determination of the band parameters of bulk 2H-MX_2 (M = Mo, W; X = S, Se) by angle-resolved photoemission spectroscopy *Sci. Rep.* **6** 36389
[15] Nguyen P V *et al* 2019 Visualizing electrostatic gating effects in two-dimensional heterostructures *Nature* **572** 220–3
[16] Miwa J A, Dendzik M, Grønborg S S, Bianchi M, Lauritsen J V, Hofmann P and Ulstrup S 2015 Van der Waals epitaxy of two-dimensional MoS_2–graphene heterostructures in ultrahigh vacuum *ACS Nano* **9** 6502–10
[17] Dau M T *et al* 2019 van der Waals epitaxy of Mn-doped $MoSe_2$ on mica *APL Mater.* **7** 051111
[18] Salazar R *et al* 2022 Visualizing giant ferroelectric gating effects in large-scale WSe_2/$BiFeO_3$ heterostructures *Nano Lett.* **22** 9260–7
[19] Mallet P, Chiapello F, Okuno H, Boukari H, Jamet M and Veuillen J-Y 2020 Bound hole states associated to individual vanadium atoms incorporated into monolayer WSe_2 *Phys. Rev. Lett.* **125** 036802
[20] Dosenovic D *et al* 2023 Mapping domain junctions using 4D-STEM: toward controlled properties of epitaxially grown transition metal dichalcogenide monolayers *2D Mater.* **10** 045024
[21] Amorim B 2018 General theoretical description of angle-resolved photoemission spectroscopy of van der Waals structures *Phys. Rev. B* **97** 165414
[22] Ebert H, Ködderitzsch D and Minár J 2011 Calculating condensed matter properties using the KKR-Green's function method—recent developments and applications *Rep. Prog. Phys.* **74** 096501
[23] Zhang Y, Xie X, Zong J, Chen W, Yu F, Tian Q, Meng Q, Wang C and Zhang Y 2021 Charge transfer between the epitaxial monolayer WSe_2 films and graphene substrates *Appl. Phys. Lett.* **119** 111602
[24] Watson M D, Date M, Louat A and Schröter N B M 2024 Novel electronic structures from anomalous stackings in NbS_2 and MoS_2 *Phys. Rev. B* **110** L121121
[25] Louie S G, Thiry P, Pinchaux R, Pétroff Y, Chandesris D and Lecante J 1980 Periodic oscillations of the frequency-dependent photoelectric cross sections of surface states: theory and experiment *Phys. Rev. Lett.* **44** 549–53
[26] Hofmann P, Søndergaard C, Agergaard S, Hoffmann S V, Gayone J E, Zampieri G, Lizzit S and Baraldi A 2002 Unexpected surface sensitivity at high energies in angle-resolved photoemission *Phys. Rev. B* **66** 245422
[27] Lobo J and Mascaraque A 2006 Observation of the noble-metal L-gap surface state in Cu(311) *J. Phys.: Condens. Matter* **18** L395
[28] Schutte W J, De Boer J L and Jellinek F 1987 Crystal structures of tungsten disulfide and diselenide *J. Solid State Chem.* **70** 207–9
[29] Pescia D, Law A R, Johnson M T and Hughes H P 1985 Determination of observable conduction band symmetry in angle-resolved electron spectroscopies: non-symmorphic space groups *Solid State Commun.* **56** 809–12
[30] Ohta T, Bostwick A, McChesney J L, Seyller T, Horn K and Rotenberg E 2007 Interlayer interaction and electronic screening in multilayer graphene investigated with angle-resolved photoemission spectroscopy *Phys. Rev. Lett.* **98** 206802
[31] Strocov V N 2018 Photoemission response of 2D electron states *J. Electron Spectrosc. Relat. Phenom.* **229** 100–7
[32] Moser S 2017 An experimentalist's guide to the matrix element in angle resolved photoemission *J. Electron Spectrosc. Relat. Phenom.* **214** 29–52
[33] Braun J, Minár J and Ebert H 2018 Correlation, temperature and disorder: recent developments in the one-step description of angle-resolved photoemission *Phys. Rep.* **740** 1–34
[34] Salazar R 2024 Raphael Salazar/Arpestb.GitLab (available at: https://gitlab.com/SLZ_Raph/arpestb)
[35] Cappelluti E, Roldán R, Silva-Guillén J A, Ordejón P and Guinea F 2013 Tight-binding model and direct-gap/indirect-gap transition in single-layer and multilayer MoS_2 *Phys. Rev. B* **88** 075409

[36] Roldán R, López-Sancho M P, Guinea F, Cappelluti E, Silva-Guillén J A and Ordejón P 2014 Momentum dependence of spin–orbit interaction effects in single-layer and multi-layer transition metal dichalcogenides *2D Mater.* **1** 034003
[37] Fang S, Defo R K, Shirodkar S N, Lieu S, Tritsaris G A and Kaxiras E 2015 Ab initio tight-binding Hamiltonian for transition metal dichalcogenides *Phys. Rev. B* **92** 205108
[38] Silva-Guillen J A, San-Jose P and Roldan R 2016 Electronic band structure of transition metal dichalcogenides from ab initio and Slater–Koster tight-binding model *Appl. Sci.* **6** 284
[39] Mak K F, Lee C, Hone J, Shan J and Heinz T F 2010 Atomically thin MoS_2: a new direct-gap semiconductor *Phys. Rev. Lett.* **105** 136805
[40] Radisavljevic B, Radenovic A, Brivio J, Giacometti V and Kis A 2011 Single-layer MoS_2 transistors *Nat. Nanotechnol.* **6** 147–50